Check for updates

Organic metal matrix Mil-88a nano-enzyme for joint repair in the osteoarthritis mouse model

Hao Hu, Xu Huang, Yankun Dai, Kairun Zhu, Xuwen Ye, Shengdong Meng, Qing Zhang and Xueguan Xie*

Huai'an Second People's Hospital, Huaian, China

Introduction: In this paper we tried to conduct a novel nanomaterial strategy to overcome osteoarthritis (OA) in a mouse model.

Methods: In this regard, after synthesizing the Mil-88a nanozyme, as a certain Fe-MOF, its toxic effects were detected by CCK-8 method and live-dead staining. The OA model of mouse was constructed, and paraffin sections of joints were taken for histological evaluation. In addition, immunofluorescence and immunohistochemistry were used to identify the OA progression and OARSI was used to evaluate the OA grades. We observed that Mil-88a could be easily synthesized and has high biocompatibility.

Results: We observed that Mil-88a could significantly promote the expression of OA anabolism-related genes such as *Col2* and also significantly inhibit the expression of OA catabolism-related genes *MMP13*. Besides, we observed better OARSI score in animals treated with Mil-88a nano-enzyme loading on organic metal matrix.

Discussion: Overall, Mil-88a nano-enzyme could be used as a novel strategy to treat OA.

Introduction

Osteoarthritis (OA) is also known as degenerative bone disease, and its clinical symptoms are usually manifested as joint swelling and pain, limited mobility, etc., and even lead to joint deformity and muscle atrophy (Wang et al., 2020). Clinically, the symptomatic treatment for OA is to mainly relieve pain and reduce deformity (Zhang et al., 2019). At present, a large number of basic research studies have carried out a closer understanding of the occurrence and development of OA, but its specific pathogenesis is still unclear. It is mainly believed that the most important reason for the pathogenesis of OA is the imbalance of reactive oxygen species (ROS) (Ding et al., 2020).

Reactive oxygen species (ROS) are known to be essential to cellular processes and are essential byproducts of cell metabolism, including superoxide anions ($O_2\bullet$), hydrogen peroxide (H_2O_2), and hydroxyl radicals ($\bullet OH$) (Tsvetkov et al., 2022). ROS typically play a key role in the regulation of cell signaling pathways that normally control cell proliferation, growth, cycle, and death (Yi et al., 2021). ROS break the structure of signaling proteins by oxidizing redox-reactive residues on proteins, leading to the regulation of protein function (Gaurav et al., 2021). However, due to the oxidation of proteins, DNA, and membrane lipids, excess ROS may be a major cause of various inflammatory diseases (Zhai et al., 2021). Strategies to remove ROS by

antioxidant molecules such as vitamins or natural enzymes such as superoxide dismutase (SOD) when the anti-ROS system is disrupted have a wide range of effects (Sun et al., 2018).

Spectroscopic capabilities have been shown to be effective biological therapeutic agents to combat oxidative stress in the treatment of various inflammatory diseases (Li et al., 2022). While there is promise in reducing ROS levels, many conventional antioxidant molecular treatments are less efficient than natural enzymes (He et al., 2020). At the same time, natural enzymes are subjected to many limitations, such as sensitivity to environmental conditions, limited functional stability, and difficulty in large-scale production (Li et al., 2017; Chen et al., 2018; Wan et al., 2020; Zhang et al., 2023). Recently, with the rapid and significant advances in nanotechnology, a series of biocatalytic or antioxidant nanostructures have been designed with unique ROS-scavenging capabilities, demonstrating promising activity to overcome these core challenges in clinical anti-ROS and anti-oxidation (Chen et al., 2020; Shetty et al., 2021). This is compared to conventional anti-inflammatory drugs, where biocatalytic or antioxidant nanostructures can achieve anti-inflammatory effects by eliminating a broad spectrum of reactive oxygen species, rather than targeting only specific inflammatory pathways or molecules, which may provide better therapeutic efficiency and greater biosafety than current clinical drugs (Zhang et al., 2018; Zhu et al., 2020; Cheng et al., 2021).

Thus, the idea of using biocatalytic or antioxidant nanostructures opens up new avenues for ROS clearance of ROS-related biotherapeutics, such as metal–organic framework (MOF) and polyphenol nanoparticles. Overall, biocatalytic or antioxidant nanostructures exhibit significant advantages, such as a remarkable ROS-scavenging capacity compared to natural enzymes, a broad spectrum of ROS elimination activity, robust stability in physiological environments, and satisfactory biocompatibility and biosafety (Li et al., 2020).

Eventually, we can regulate ROS levels to treat inflammatory diseases. It has also been reported that MOF nanoparticles have the ability to remove reactive oxygen species (Bian et al., 2020). ROS cleared by MOFs is a promising candidate for therapeutic applications due to its high biocompatibility, 3D matrix, and modification capabilities. Therefore, a novel, safe, and effective drug targeting ROS imbalance needs to be developed urgently. Nanozyme is a kind of nanomaterial with enzymatic activity similar to proteins. Mil-88a belongs to the family of metal–organic framework (MOF) nanozyme with peroxidase mimetic activity and good biocompatibility (Kasula et al., 2022) and thus is considered to be a promising nano-enzyme repair system for promoting OA repair. This study investigated the role of Mil-88a nanozyme co-loaded with the organic metal matrix in promoting OA repair in a mouse model.

Materials and methods

Material synthesis

The preparation process of Mil-88a was carried out based on the improved techniques of the existing literature (Gaurav et al., 2021; Yi et al., 2021). First of all, 0.9744 g (8.4 mmol) fumaric acid and 2.2722 g (8.4 mmol) $FeCl_3$ were weighed. Then, the mixture was dissolved in 42 mL ultrapure water and stirred for 2 h. The solution was placed in the reaction kettle in a blast drying oven and then in a drying oven. The reaction was carried out at 85°C for 2 h. The reactor was taken out

and cooled to room temperature. After the reaction kettle was cooled, the solution was centrifuged at 10,000 rpm for 10 min to obtain a brick-red solid. The precipitate was washed three times with absolute ethanol and dried in a vacuum drying oven at 100°C for 6 h. Ultimately, the solid obtained by drying was the metal–organic framework Mil-88a and was stored for future use.

Characterization of Mil-88a

The aforementioned dried precipitate was used for SEM, XRD, TGA, and FTIR characterization. In addition, a small amount of the powder was ultrasonically dispersed in ultrapure water for particle size analysis by DLS.

Detection of the SOD clearance rate of Mil-88a

Using the principle of the xanthine oxidase system to generate superoxide anion, according to the kit instructions (Beijing Solarbio Science & Technology Co., 100T/48S), the WST working solution and the enzyme working solution were prepared, respectively. A small amount of the sample powder was prepared as the mother solution, and then different proportions of the mother solution were mixed with pure water in a 1.5-mL tube to obtain sample solutions of different concentrations. The solution was incubated at 37°C for 20 min and was fully centrifuged to remove the material. The absorbance at 450 nm of the supernatant was measured, calculated, and compared with the control group, and the process was repeated three times for each group.

Detection of the hydroxyl radical-scavenging rate of Mil-88a

Using the principle that hydroxyl radicals are generated by the Fenton reaction and the interaction between hydroxyl radicals and chromogenic reagents (BOXBIO, AKAO013M), different concentrations of Mil-88a solutions were prepared according to the kit instructions, and the hydroxyl radical-scavenging efficiency of Mil-88a at different concentrations was measured. The process was repeated three times.

Primary culture of chondrocytes

Cartilage tissue was isolated from 5-day-old SD rats and washed with PBS containing 10% double antibody to remove blood clots. After incubation with 0.25% trypsin for 1.5 h at 37°C, 0.02% type II collagenase was replaced with 0.02% collagenase overnight to separate free cells. After the dissociated cells adhered to the wall, the medium was changed every 2 days and passed to the P3–P5 generation for use.

Biocompatibility testing

CCK-8 method: A density of 5×10^4 P3–P5 chondrocytes was inoculated in a 96-well plate overnight. After the cells adhered to the

wall, the medium was changed and 100 μL, 1 μg/mL, and 2 μg/mL chondrocytes were added, respectively. Mil-88a was resuspended in 0.25 mL of fresh media to get different concentrations (0 μg/mL, 1 μg/mL, 2 μg/mL, 5 μg/mL, 10 μg/mL, 20 μg/mL, 50 μg/mL, and 100 μg/mL). After allowing culturing in the cell incubator for 24 h, the medium was completely removed and rinsed with PBS twice to completely remove the material. A measure of 110 μL of CCK-8 containing the medium prepared at a ratio of 1:10 was added and incubated at 37°C for 1 h. After incubation, the supernatant medium was carefully pipetted to a new 96-well plate, and the absorbance at 450 nm was measured using a microplate reader. Then, the process was repeated three times per set. Staining of live and dead cells: A total of 5,000 P3–P5 chondrocytes were seeded in a 96-well plate overnight, and then the original medium was replaced by 0.2 mL of the fresh medium containing different concentrations of Mil-88a (0 μg/mL, 1 μg/mL, 2 μg/mL, 5 μg/mL, 10 μg/mL, 20 μg/mL, 50 μg/mL, and 100 μg/mL) for 24 h. The medium was removed and washed two times with PBS. A measure of 100 μL of calcein-AM/PI staining working solution was added in the dark for 20 min, PBS was used to remove excess dye, and three fields of view were randomly selected for observation under a confocal microscope at ×100 magnification.

PCR detection

A density of 3×10^5 cells per well was inoculated in a six-well plate, and after culturing for 24 h, the old medium was removed and washed thoroughly with PBS, and then 1 mL of H_2O_2 induction solution prepared in a serum-free medium with a concentration of 450 μmol/L was added. After the cells were fully induced, equal volumes of Mil-88a solutions prepared with the serum-free medium of different concentrations were added, and culturing was continued for 24 h. Subsequently, the medium containing nanomaterials was removed by thorough rinsing with PBS. Ultimately, RNA was extracted for PCR experiments.

Immunofluorescence

Each well was seeded with 75,000 chondrocytes of the same generation in a 24-well plate that had been placed on the slides. After adhering overnight, the cells were induced by oxidative stress in 0.25 mL of the serum-free medium mixed with H_2O_2 for 20 min. Then, the serum-free medium was replaced by 0.25 mL of the fresh medium containing different concentrations of Mil-88a (0 μg/mL, 1 μg/mL, 2 μg/mL, 5 μg/mL, 10 μg/mL, 20 μg/mL, 50 μg/mL, and 100 μg/mL). The treated cells were incubated for another 24 h, and it was washed three times with PBS buffer, fixed with 4% paraformaldehyde for 25 min, washed with PBS three times, then incubated with 3% H_2O_2 for 15 min, washed with PBS three times, and then incubated with goat serum for 30 min. After the blocking treatment, the diluted IL-1β primary antibody (1:200) was added dropwise to the slides and incubated overnight in a refrigerator at 4°C. Subsequently, the cells were incubated with biotinylated goat anti-rabbit secondary antibody (1:500) and allowed dilution for 1 h. Finally, the nuclei were labeled with 4′,6-diamidino-2-phenylindole (DAPI), incubated in the dark for 10 min, washed with buffer three times, dried the water on the slide, and sealed with neutral resin. After slicing, the sections were observed and photographed using a fluorescence microscope.

OARSI score

In this study, the Osteoarthritis Research Society International (OARSI) score was used to evaluate the degree of articular cartilage degeneration (Chen et al., 2018). OARSI grade (grade) is divided into six grades, and the higher the score, the more serious the cartilage degeneration. Grade 0: normal, with normal cartilage surface and chondrocytes; grade 1: slight fibrosis on the articular cartilage surface, unevenness, but no cartilage loss, and no involvement but middle and deep cartilage; grade 2: fissures on the articular cartilage surface and cartilage loss, the middle layer of cartilage is involved, fibrosis, chondrocyte proliferation and death, abnormal cartilage matrix staining, etc.; grade 3: the fissure involves the deep cartilage, and chondrocyte death and proliferation are mainly distributed along the fissure; grade 4: the matrix around the fissure is lost and articular cartilage erosion; grade 5: articular cartilage erosion, full-thickness erosion of unmineralized hyaline cartilage, mineralized cartilage, and subchondral bone exposed on the articular surface; grade 6: joint deformation, articular surface fibrocartilage, osteophyte formation, etc. In this study, the OARSI score was independently completed by two sports medicine doctors with clinical work experience under the light microscope (×100) according to the scoring rules, and the average score was taken as the final score, and the sample grouping was not informed.
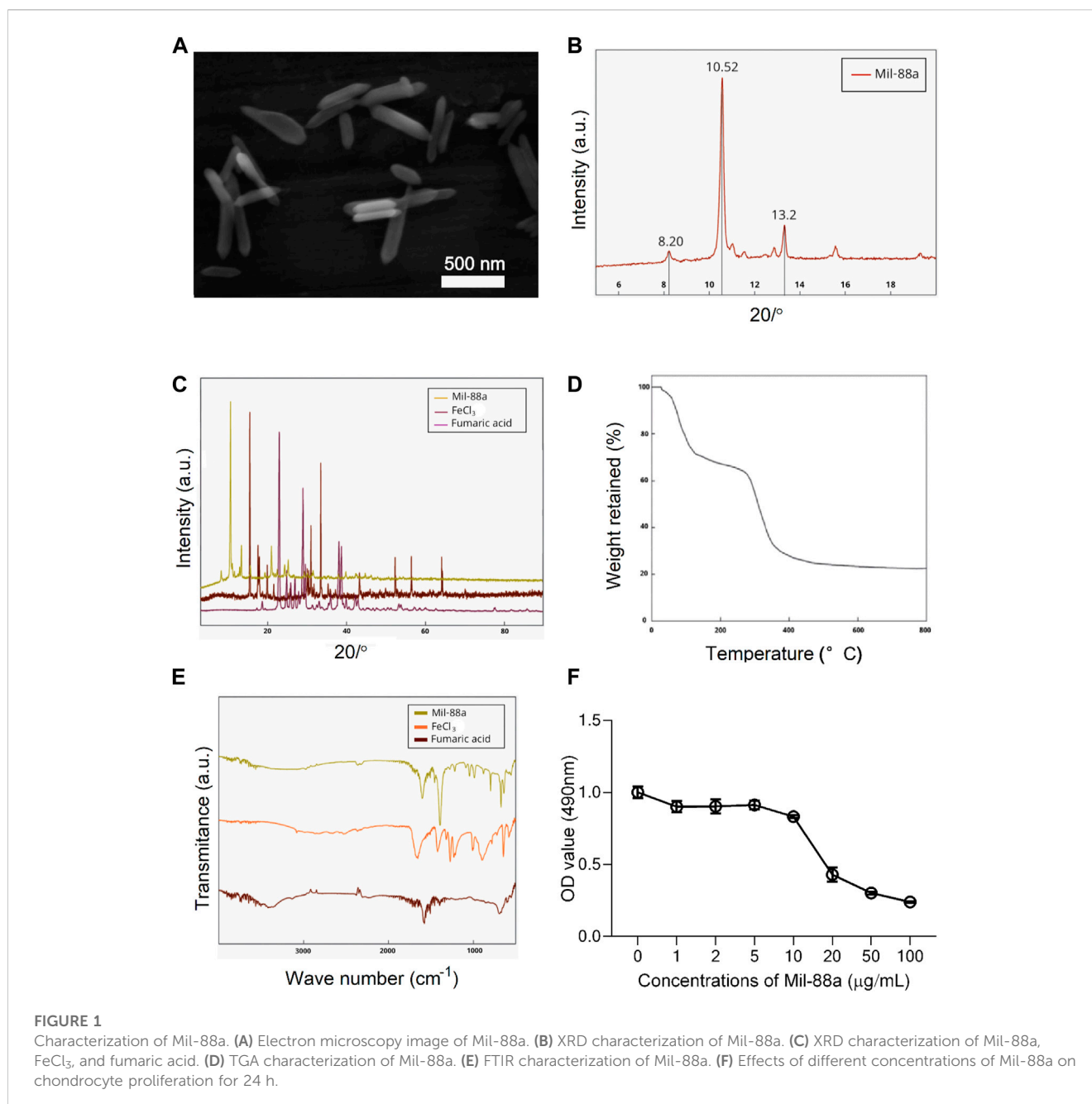
Statistical analysis

SPSS and GraphPad Prism statistical software were used to analyze data, measurement data were expressed as mean ± standard deviation ($\bar{x} \pm s$), and a t-test was used for the comparison between groups. Comparisons among multiple groups were performed using one-way analysis of variance (ANOVA). $p < 0.05$ was regarded as a statistically significant difference.

Results

Evaluating Mil-88a by scanning electron microscopy and characterization by XRD, TGA, and FTIR

Electron microscopy showed that the synthesized Mil-88a was in the shape of hexagonal rods, as shown in Figure 1A. The overall main peak of Mil-88a did not show a large shift in the whole spectrum. There were three characteristic peaks in the range of 6°–15°, which were 2.8°, 10.4°, and 12.9°, respectively, as shown in Figures 1B and C. The mass retention of Mil-88a was basically unchanged in the range of 100°C–300°C. FTIR showed that Mil-88a had all the characteristic peaks of $FeCl_3$ and fumaric acid, as shown in Figures 1D, E. Next, the size of Mil-88a was characterized by dynamic light scattering (DLS) analysis, which demonstrated an ideal and uniform morphology with an average diameter of approximately 100 nm (Supplementary Figure S1).

FIGURE 1
Characterization of Mil-88a. **(A)** Electron microscopy image of Mil-88a. **(B)** XRD characterization of Mil-88a. **(C)** XRD characterization of Mil-88a, FeCl$_3$, and fumaric acid. **(D)** TGA characterization of Mil-88a. **(E)** FTIR characterization of Mil-88a. **(F)** Effects of different concentrations of Mil-88a on chondrocyte proliferation for 24 h.

Biocompatibility evaluation of Mil-88a

CCK-8 method: When the concentration of Mil-88a was in the range of 1–10 μg/mL, the chondrocyte survival rate was maintained above 80%, as shown in Figure 1F. Staining of live and dead cells: When the concentration was greater than 10 μg/mL, it showed strong toxicity to chondrocytes ($p < 0.001$), as shown in Figures 2A, B. ROS-scavenging effect of Mil-88a: With the increase in the Mil-88a concentration, the SOD-scavenging rate of Mil-88a gradually increased ($p < 0.001$; Figure 2C), and the hydroxyl radical-scavenging rate was different from that of Fe$_3$O$_4$, but the scavenging efficiency did not change with Mil-88a ($p < 0.05$,

Figure 2D). This phenomenon takes place because when the nanoreactor reaches the tumor site, a high concentration of glutathione reduces Fe^{3+}, triggering the structural collapse of MOF and the release of Fe^{2+}, while GOx catalyzes the oxidation of glucose to H$_2$O$_2$. Then, the Fenton reaction occurs between H$_2$O$_2$ and Fe^{2+}, producing the hydroxyl radical (•OH). Therefore, after Mil-88a, as a Fe-MOF, is taken up by cells, SOD is only consumed and •OH is consumed and increased. In addition, we evaluated the expression of IL-1β to figure out the effect of Mil-88a on pro-inflammatory cytokines (Figure 2E; Supplementary Figure S2). We observed that Mil-88a could significantly decrease the expression of IL-1β in a dose-dependent manner.
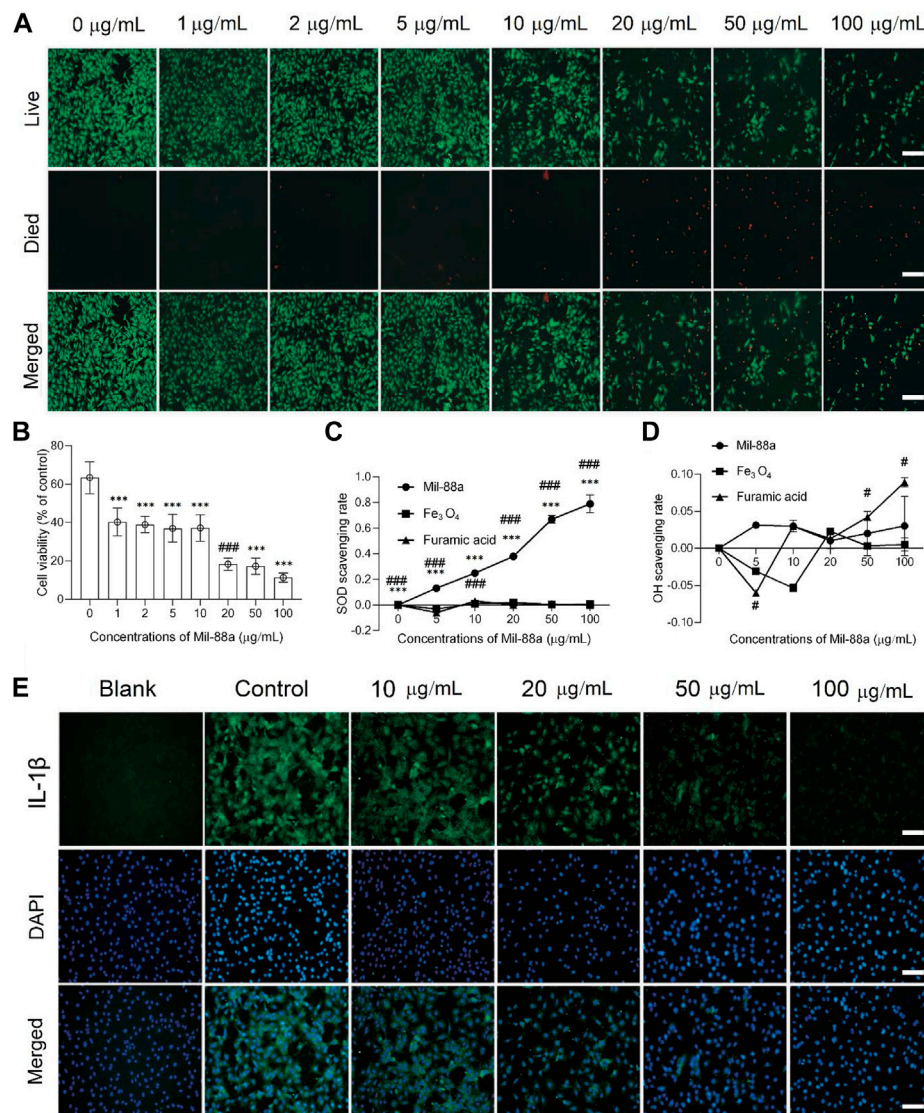
FIGURE 2
Cytotoxicity and biocompatibility testing of Mil-88a *in vitro*. **(A)** Fluorescence microscopy images of calcein-AM/PI staining in cells treated with different concentrations of Mil-88a (1, 2, 5, 10, 20, 50, and 100 μg/mL). Live, live cells (green); died, dead cells (red); merge, overlay. **(B)** Cell viabilities of chondrocyte cells treated with different concentrations of Mil-88a (1, 2, 5, 10, 20, 50, and 100 μg/mL and $n = 4$). The effects of different concentrations of Mil-88a (1, 2, 5, 10, 20, 50, and 100 μg/mL and $n = 4$) on SOD- **(C)** and OH- **(D)** scavenging rates for 24 h, and IL-1β **(E)**. ***$p < 0.001$ compared with 0 μg/mL; ###$p < 0.001$ compared with 10 μg/mL. Scale bar = 100 μm.

Mil-88a alleviated the pathological manifestations of OA *in vivo*

To explore the effect of Mil-88a nano-enzyme on the osteoarthritis mouse model, Mil-88a nano-enzyme was administered by local injection into the joint cavity. Safranin O staining of paraffin sections of rat knee joints showed that rats on a high-cholesterol diet showed a more severe OA phenotype than those on a normal diet (Figure 3A). The joint surface was not smooth, the safranin O staining and immunohistochemical staining intensity of type II collagen (col2) decreased, and the immunohistochemical staining intensity of MMP13 (matrix metalloproteinases 13) increased, indicating that the ECM proteoglycan content of

articular cartilage Mil-88a nano-enzyme treatment can significantly increase the content of protein polysaccharide and type II collagen, effectively improve the degenerative lesions of the aforementioned knee cartilage tissue, and alleviate the progression of OA (Figure 3A). The severity of OA in the mouse was scored using the OARSI score. The results showed that the OARSI scores of MTP (Figure 3B) and MFC (Figure 3C) of the animals treated with Mil-88a were significantly lower than those of the animals in the non-treated group. This indicated that the degenerative lesions of the cartilage tissue in the Mil-88a-treated group were milder. Scoring of Col2 (Figure 3D) and MMP13 (Figure 3E) immunohistochemistry also showed this trend. The results suggest that Mil-88a could alleviate the progression of OA.
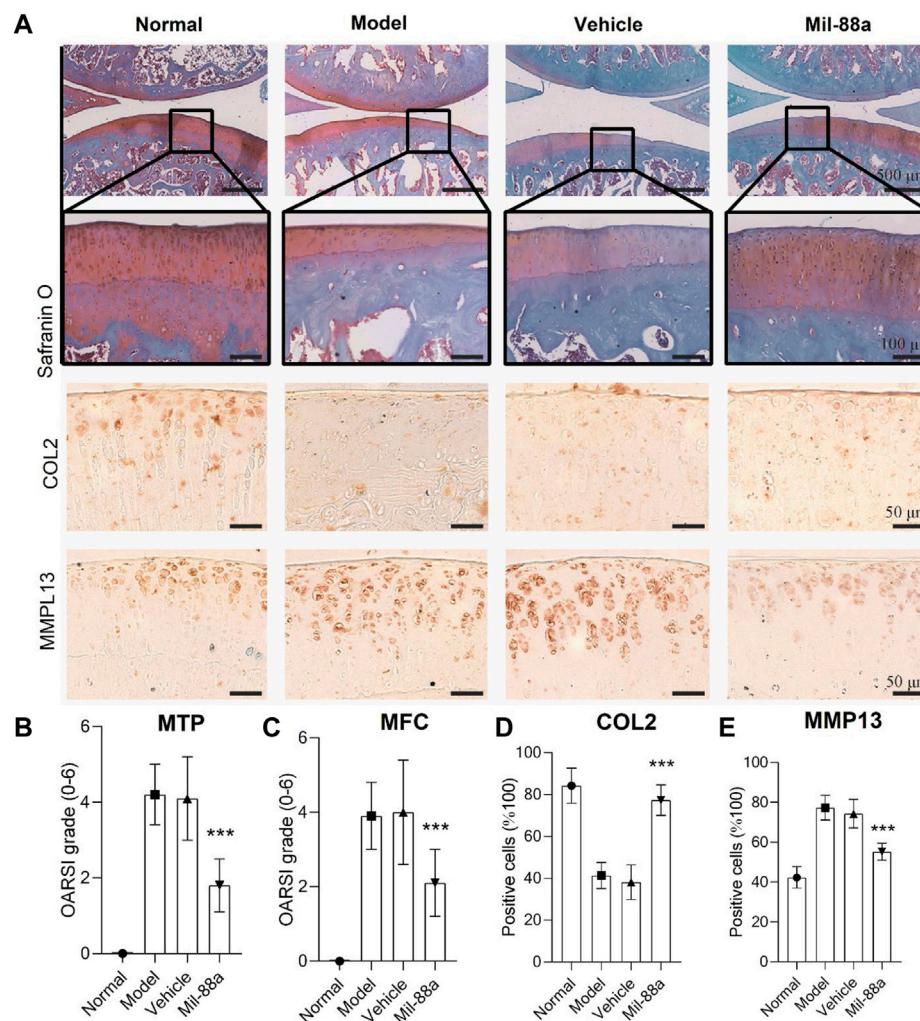
FIGURE 3
Mil-88a alleviates the pathological manifestations of OA. **(A)** Safranin O staining of paraffin sections of rat knee tissue, scale bar = 500 or 100 μm, and immunohistochemical staining of Col2 and MMP13, scale bar = 50 μm. **(B, C)** OARSI score. **(D, E)** Positive cell statistics of Col2 and MMP13. (n = 6). ns, no statistical difference; $*p < 0.05$; $**p < 0.01$; $***p < 0.001$.

Evaluation of the effect

In this section, we first tried to evaluate the conduction of OA in the mouse model using luminescence imaging (Figures 4A, B, 5). We observed high intensity of luminescence in the joints with the conduction of OA in comparison to normal mice (Figure 4B). In addition, we observed a significant drop in luminescence density in joints treated with Mil-88a. These results suggested that Mil-88a could improve OA *in vivo*. In addition, we applied a micro-CT scan to assess the effect of Mil-88a on bone density (Figures 4C, D). Dramatically, we observed that Mil-88a could increase bone density at the site of femoral joints (Figures 4E–H). These results suggested that Mil-88a could significantly increase bone formation to improve OA.

Discussion

Approximately 16.2% of patients in China suffer from OA for a long time. The unbearable pain and extremely high

disability rate seriously affect the quality of life of patients and destroy the stability of families and society (Xu et al., 2022). Although a lot of basic research has been carried out, the etiology and pathogenesis of OA are still inconclusive, and it is mainly believed to be related to factors such as age, occupation, strain, and endocrine (Lan et al., 2019; Qiu et al., 2020). Excessive ROS is the cause of arthritis inflammatory lesions. One of the important factors, as a potential target for the treatment of OA, is how to reverse the ROS imbalance, which has become the key to curing OA (Hou et al., 2021). MOFs are nanoparticles with a special 3D network structure formed by the self-assembly of metal nodes and organic ligands through chemical bonds. With a large specific surface area, adjustable pore size, and stable physicochemical properties, it is considered a promising biomimetic nanozyme (Xiong et al., 2022). Wu et al. (Zhou et al., 2022) reported that the special metal node structure of MOFs has oxidase analog activity, which is considered an ideal nanozyme for scavenging ROS. In this study, electron microscopy of Mil-88a showed a hexagonal rod shape, and XRD showed three characteristic peaks
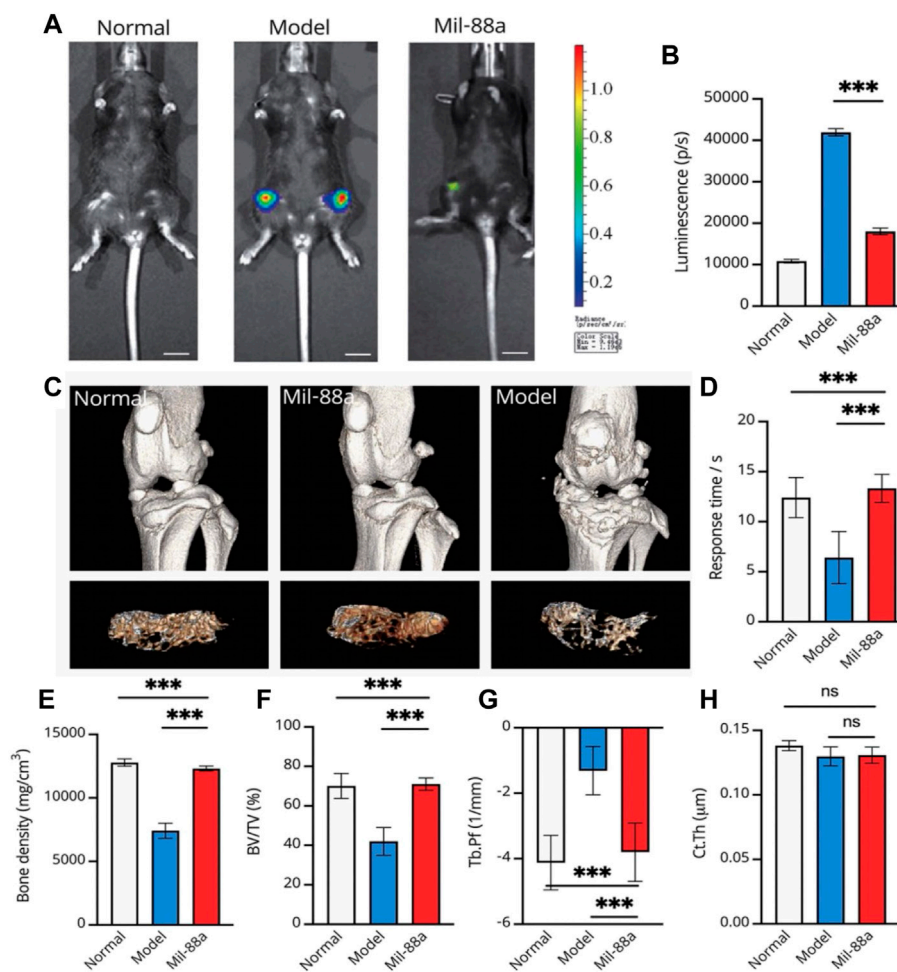
FIGURE 4
Representative luminescence imaging *in vivo* and evaluation of bone density in the mouse joint using micro-CT. Evaluation of osteoarthritis using luminescence imaging **(A, B)**. The 3D reconstruction of CT indicates the bone changes, and the tibial plateau section shows the structure of bone trabeculae **(C)**. For evaluating the response time, mice were placed on the heating platform at 55°C, and the reaction time of licking and jumping was shown; a micro-CT scan of the joints of mice was performed **(C, D)**. Bone density (mg/cm^3) **(E)**, bone volume fraction (BV/TV) **(F)**, trabecular pattern factor (Tb.Pf, 1/mm) **(G)**, and cortical bone thickness **(H)** were used to assess subchondral bone changes in osteoarthritis by quantitative CT. Values were presented as mean $\pm$ SD. ***$p < 0.001$ ($n = 5$).

in the range of 6°–15°, which was consistent with the previous report (Chen et al., 2022). FTIR has all the characteristic peaks of raw materials, and TGA confirms that Mil-88a still has good stability in the range of approximately 100°C–300°C. In order to verify the cytotoxicity of Mil-88a, CCK-8 and live–dead staining indicated that when the concentration of Mil-88a was less than 10 μg/mL, there was basically no cytotoxicity ($p < 0.001$). In conclusion, Mil-88a was successfully synthesized with good biocompatibility. OA is mainly manifested as a cartilage defect. Reducing the oxidative stress of chondrocytes and removing excess reactive oxygen species will be beneficial to the regeneration of cartilage (He et al., 2021; Ma et al., 2022). ROS include SOD and OH (Chen et al., 2021). The ROS clearance rate of Mil-88a was further verified. The results showed that the SOD clearance rate of Mil-88 was concentration-dependent,

and the OH clearance rate did not change with the concentration but was still higher than that of Fe_3O_4 ($p < 0.05$), suggesting that it is not simply due to its porous physical structure that scavenges ROS and the specific mechanism remains to be further studied. The results suggested that Mil-88a has the potential to act as a ROS-scavenging nanozyme in the joint cavity. ROS is an important signaling molecule that regulates inflammation. The imbalance of ROS leads to the abnormal expression of TNF-α and IL-1β inflammatory factors. Previous works of literature reported that TNF-α and IL-1β are closely related to cartilage destruction and the occurrence of synovitis (Ma et al., 2020; Cao et al., 2023). TNF-α, as a key inhibitor of cartilage collagen production, promotes the apoptosis of chondrocytes, and the activation of TNF-α causes the occurrence of the inflammatory cascade by upregulating the inflammatory trigger of IL-1β (Liu et al., 2021; Peng et al., 2021).
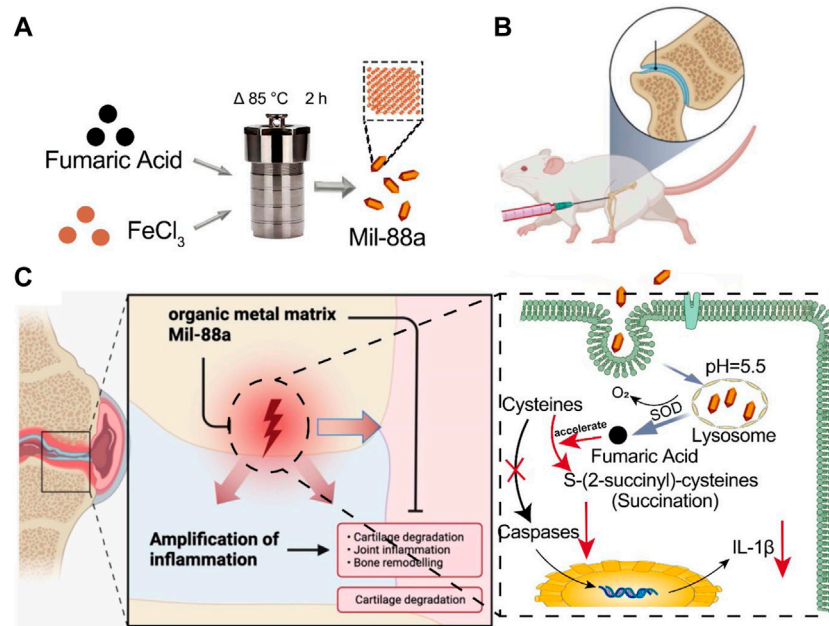
FIGURE 5
Schematic of how Mil-88a could improve OA in a mouse model. **(A)** Flow diagram of the prepared Mil-88a. **(B)** Illustration of the injected method of Mil-88a. **(C)** The treatment process for suppressing the expression of IL-1β and relief of inflammatory response.

Conclusion

In summary, we synthesized a novel platform based on Fe-MOF (Mil-88a) to overcome osteoarthritis (OA), which has good biosafety and can downregulate the expression of oxidative and inflammatory factors in OA-induced chondrocytes. In this regard, after synthesizing the Mil-88a nanozyme, its toxic effects were detected by the CCK-8 method and live–dead staining. The OA mouse model was constructed, and paraffin sections of the joints were obtained for histological evaluation. In addition, immunofluorescence and immunohistochemistry were used to identify the OA progression, and the OARSI score was used to evaluate the OA grades. We observed that Mil-88a could be easily synthesized and has high biocompatibility. We observed that Mil-88a could significantly promote the expression of OA anabolism-related genes such as *Col2* and also significantly inhibit the expression of OA catabolism-related genes such as *MMP13*. In addition, we observed better OARSI scores in animals treated with Mil-88a nano-enzyme loaded on the organic metal matrix. Overall, Mil-88a co-loaded with the organic metal matrix could be used as a novel nano-enzyme strategy in the treatment of OA. We also observed that Mil-88a nanozyme could significantly improve OARSI scores and OA in the mouse model in this study. Thus, our Mil-88a might be

particularly meaningful and readily adapted to OA in a broad diversity of the current situation.

Data availability statement

The raw data supporting the conclusion of this article will be made available by the authors, without undue reservation.

Ethics statement

The animal study was reviewed and approved by Huai'an Second People's Hospital.

Author contributions

XX and HH conceived the presented idea and together with XH designed the experiment. YD and KZ carried out most of the experiments. XY and SM contributed to sample preparation and data analysis. QZ wrote the manuscript. All authors discussed the results, provided critical feedback, and contributed to the final manuscript.

Conflict of interest

The authors declare that the research was conducted in the absence of any commercial or financial relationships that could be construed as a potential conflict of interest.

Publisher's note

All claims expressed in this article are solely those of the authors and do not necessarily represent those of their affiliated organizations, or those of the publisher, the editors, and the reviewers. Any product that may be evaluated in this article, or claim that may be made by its manufacturer, is not guaranteed or endorsed by the publisher.

Supplementary material

The Supplementary Material for this article can be found online at: https://www.frontiersin.org/articles/10.3389/fbioe.2023.1164942/full#supplementary-material

References

Bian, Y., Liu, B., Liang, S., Ding, B., Zhao, Y., Jiang, F., et al. (2020). Cu-based MOFs decorated dendritic mesoporous silica as tumor microenvironment responsive nanoreactor for enhanced tumor multimodal therapy. *Chem. Eng. J.* 435, 135046. doi:10.1016/j.cej.2022.135046

Cao, Z., Wang, H., Chen, J., Zhang, Y., Mo, Q., Zhang, P., et al. (2023). Silk-based hydrogel incorporated with metal-organic framework nanozymes for enhanced osteochondral regeneration. *Bioact. Mater.* 20, 221–242. doi:10.1016/j.bioactmat.2022.05.025

Chen, C., Wang, Z., Jia, S., Zhang, Y., Ji, S., Zhao, Z., et al. (2020). Evoking highly immunogenic ferroptosis aided by intramolecular motion-induced photo-hyperthermia for cancer therapy. *Adv. Sci.* 9, e2104885. doi:10.1002/advs.202104885

Chen, J., Wei, X., Tang, H., Munyemana, J. C., Guan, M., Zhang, S., et al. (2021). Deep eutectic solvents-assisted synthesis of ZnCo2O4 nanosheets as peroxidase-like nanozyme and its application in colorimetric logic gate. *Talanta* 222, 121680. doi:10.1016/j.talanta.2020.121680

Chen, S., Jia, Q., Zheng, X., Wen, Y., Liu, W., Zhang, H., et al. (2018). PEGylated carbon dot/MnO$_2$ nanohybrid: A new pH/H$_2$O$_2$-driven, turn-on cancer nanotheranostics. *Sci. China Mater.* 61, 1325–1338. doi:10.1007/s40843-018-9261-x

Chen, Y., Wang, Y., Chen, Z., Cai, J., Li, K., Huang, H., et al. (2022). NIR-driven polydopamine-based nano-enzymes as ROS scavengers to suppress osteoarthritis progression. *Mater. Today Nano* 19, 100240. doi:10.1016/j.mtnano.2022.100240

Cheng, Y., Wen, C., Sun, Y. Q., Yu, H., and Yin, X. B. (2021). Mixed-metal MOF-derived hollow porous nanocomposite for trimodality imaging guided reactive oxygen species-augmented synergistic therapy. *Adv. Funct. Mater.* 31 (37), 2104378. doi:10.1002/adfm.202104378

Ding, S. S., He, L., Bian, X. W., and Tian, G. (2020). Metal-organic frameworks-based nanozymes for combined cancer therapy. *Nano Today* 35, 100920. doi:10.1016/j.nantod.2020.100920

Gaurav, K., Nirmal, P., Venkateswaran, V., and Sang-Jae, K. (2021). Biodegradable metal-organic framework MIL-88A for triboelectric nanogenerator. *iScience* 24, 102064. doi:10.1016/j.isci.2021.102064

He, H., Du, L., Guo, H., An, Y., Lu, L., Chen, Y., et al. (2020). Redox responsive metal organic framework nanoparticles induces ferroptosis for cancer therapy. *Small* 16, 2001251. doi:10.1002/smll.202001251

He, S. B., Yang, L., Lin, M. T., Noreldeen, H. A., Yu, R. X., Peng, H. P., et al. (2021). Acetaminophen sensor based on the oxidase-like activity and interference self-elimination ability of chondroitin sulfate-modified platinum nanozyme. *Sensors Actuators B Chem.* 347, 130627. doi:10.1016/j.snb.2021.130627

Hou, W., Ye, C., Chen, M., Gao, W., Xie, X., Wu, J., et al. (2021). Excavating bioactivities of nanozyme to remodel microenvironment for protecting chondrocytes and delaying osteoarthritis. *Bioact. Mater.* 6 (8), 2439–2451. doi:10.1016/j.bioactmat.2021.01.016

Kasula, M., Le, T., Thomsen, A., and Rabbani Esfahani, M. (2022). Silver metal organic frameworks and copper metal organic frameworks immobilized on graphene oxide for enhanced adsorption in water treatment. *Chem. Eng. J.* 439, 135542. doi:10.1016/j.cej.2022.135542

Lan, G., Ni, K., Veroneau, S. S., Luo, T., You, E., and Lin, W. 2019. Nanoscale metal-organic framework hierarchically combines high-Z components for multifarious radio-enhancement. *J. Am. Chem. Soc.* 141, pp.6859–6863. doi:10.1021/jacs.9b03029

Li, C., Shen, J., Wu, K., and Yang, N. (2022). Metal centers and organic ligands determine electrochemistry of metal-organic frameworks. *Small. Mar.* 18, e2106607. doi:10.1002/smll.202106607

Li, P. X., Xie, Z. X., Jin, A. P., Li, J., and Guo, G. C. (2020). A new photochromic Gd-MOF with photoswitchable bluish-white to greenish-yellow emission based on electron transfer. *Chem. Commun. (Camb).* 56, 14689–14692. doi:10.1039/d0cc06019d

Li, S. Y., Cheng, H., Xie, B. R., Qiu, W. X., Zeng, J. Y., Li, C. X., et al. (2017). Cancer cell membrane camouflaged cascade bioreactor for cancer targeted starvation and photodynamic therapy. *ACS Nano* 11, 7006–7018. doi:10.1021/acsnano.7b02533

Liu, Y., Qing, Y., Jing, L., Zou, W., and Guo, R. (2021). Platinum–copper bimetallic colloid nanoparticle cluster nanozymes with multiple enzyme-like activities for scavenging reactive oxygen species. *Langmuir* 37 (24), 7364–7372. doi:10.1021/acs.langmuir.1c00697

Lopez-Cantu, D. O., González-González, R. B., Sharma, A., Bilal, M., Parra-Saldívar, R., and Iqbal, H. M. (2022). Bioactive material-based nanozymes with multifunctional attributes for biomedicine: Expanding antioxidant therapeutics for neuroprotection, cancer, and anti-inflammatory pathologies. *Coord. Chem. Rev.* 469, 214685. doi:10.1016/j.ccr.2022.214685

Ma, J., Qiu, J., and Wang, S. (2020). Nanozymes for catalytic cancer immunotherapy. *ACS Appl. Nano Mater.* 3 (6), 4925–4943. doi:10.1021/acsanm.0c00396

Ma, X., Hao, J., Wu, J., Li, Y., Cai, X., and Zheng, Y. (2022). Prussian blue nanozyme as a pyroptosis inhibitor alleviates neurodegeneration. *Adv. Mater.* 34 (15), 2106723. doi:10.1002/adma.202106723

Mou, X., Wu, Q., Zhang, Z., Liu, Y., Zhang, J., Zhang, C., et al. (2022). Nanozymes for regenerative medicine. *Small Methods* 6, 2200997. doi:10.1002/smtd.202200997

Peng, Y., He, D., Ge, X., Lu, Y., Chai, Y., Zhang, Y., et al. (2021). Construction of heparin-based hydrogel incorporated with Cu5.4O ultrasmall nanozymes for wound healing and inflammation inhibition. *Bioact. Mater.* 6 (10), 3109–3124. doi:10.1016/j.bioactmat.2021.02.006

Qiu, Q., Wang, T., Jing, L., Huang, K., and Qin, D. (2020). Tetra-carboxylic acid based metal-organic framework as a high-performance bifunctional electrocatalyst for HER and OER. *Int. J. Hydrogen Energy* 45, 11077–11088. doi:10.1016/j.ijhydene.2020.02.033

Rajeshri, D. P., Mihir, K. R., and Navin, R. S. (2020). Formation of Diacerein – fumaric acid eutectic as a multi-component system for the functionality enhancement. *J. Drug Deliv. Sci. Technol.* 58, 101562. doi:10.1016/j.jddst.2020.101562

Shetty, S. C., Yandrapalli, N., Pinkwart, K., Krafft, D., Vidakovic-Koch, T., Ivanov, I., et al. (2021). Directed signaling cascades in monodisperse artificial eukaryotic cells. *ACS Nano* 15, 15656–15666. doi:10.1021/acsnano.1c04219

Sun, L., Li, Y. H., and Shi, H. (2018). A ketone functionalized Gd (III)-MOF with low cytotoxicity for anti-cancer drug delivery and inhibiting human liver cancer cells. *J. Clust. Sci.* 30, 251–258. doi:10.1007/s10876-018-1482-3

Tsvetkov, P., Coy, S., Petrova, B., Dreishpoon, M., Verma, A., Abdusamad, M., et al. (2022). Copper induces cell death by targeting lipoylated TCA cycle proteins. *Sci. Mar* 18 (375), 1254–1261. doi:10.1126/science.abf0529

Wan, X., Song, L., Pan, W., Zhong, H., Li, N., and Tang, B. (2020). Tumor-targeted cascade nanoreactor based on metal–organic frameworks for synergistic ferroptosis–starvation anticancer therapy. *ACS Nano* 14, 11017–11028. doi:10.1021/acsnano.9b07789

Wang, D., Jana, D., and Zhao, Y. (2020). Metal–organic framework derived nanozymes in biomedicine. *Accounts Chem. Res.* 53 (7), 1389–1400. doi:10.1021/acs.accounts.0c00268

Wu, H., Li, F., Shao, W., Gao, J., and Ling, D. (2019). Promoting angiogenesis in oxidative diabetic wound microenvironment using a nanozyme-reinforced self-protecting hydrogel. *ACS central Sci.* 5 (3), 477–485. doi:10.1021/acscentsci.8b00850

Xiong, H., Zhao, Y., Xu, Q., Xie, X., Wu, J., Hu, B., et al. (2022). Biodegradable hollow-structured nanozymes modulate phenotypic polarization of macrophages and relieve hypoxia for treatment of osteoarthritis. *Small* 18 (32), 2203240. doi:10.1002/smll.202203240

Xu, W., Wang, T., Qian, J., Wang, J., Hou, G., Wang, Y., et al. (2022). Fe (II)-hydrazide coordinated all-active metal organic framework for photothermally enhanced tumor penetration and ferroptosis-apoptosis synergistic therapy. *Chem. Eng. J.* 437, 135311. doi:10.1016/j.cej.2022.135311

Yi, X., Ji, H., Wang, C., Li, Y., Li, Y. H., Zhao, C., et al. (2021). Photocatalysis-activated SR-AOP over PDINH/MIL-88A(Fe) composites for boosted chloroquine phosphate degradation: Performance, mechanism, pathway and DFT calculations. *Appl. Catal. B Environ.* 293, 120229. doi:10.1016/j.apcatb.2021.120229

Zhai, Y., Wang, J., Lang, T., Kong, Y., Rong, R., Cai, Y., et al. (2021). T lymphocyte membrane-decorated epigenetic nanoinducer of interferons for cancer immunotherapy. *Nat. Nanotechnol. Nov.* 16, 1271–1280. doi:10.1038/s41565-021-00972-7

Zhang, D., Wu, M., Cai, Z., Liao, N., Ke, K., Liu, H., et al. (2018). Chemotherapeutic drug based metal-organic particles for microvesicle-mediated deep penetration and programmable pH/NIR/hypoxia activated cancer photochemotherapy. *Adv. Sci.* 5, 1700648. doi:10.1002/advs.201700648

Zhang, X., Li, G., Wu, D., Li, X., Hu, N., Chen, J., et al. (2019). Recent progress in the design fabrication of metal-organic frameworks-based nanozymes and their applications to sensing and cancer therapy. *Biosens. Bioelectron.* 137, 178–198. doi:10.1016/j.bios.2019.04.061

Zhang, Z., Zhao, J., Chen, Z., Wub, H., and Wang, S. (2023). A molybdenum-based nanoplatform with multienzyme mimicking capacities for oxidative stress-induced acute liver injury treatment. *Inorg. Chem. Front.* 10, 1305–1314. doi:10.1039/d2qi02318k

Zhou, T., Ran, J., Xu, P., Shen, L., He, Y., Ye, J., et al. (2022). A hyaluronic acid/platelet-rich plasma hydrogel containing MnO2 nanozymes efficiently alleviates osteoarthritis *in vivo*. *Carbohydr. Polym.* 292, 119667. doi:10.1016/j.carbpol.2022.119667

Zhu, Y., Xin, N., Qiao, Z., Chen, S., Zeng, L., Zhang, Y., et al. (2020). Bioactive MOFs based theranostic agent for highly effective combination of multimodal imaging and chemo-phototherapy. *Adv. Healthc. Mater.* 9 (14), 2000205. doi:10.1002/adhm.202000205